Graphene-Quantum-Dot Assembled Nanotubes: A New Platform for Efficient Raman Enhancement

Huhu Cheng,[†] Yang Zhao,[†] Yueqiong Fan,[†] Xuejun Xie,[†] Liangti Qu,[†,*] and Gaoquan Shi[‡,*]

[†]Key Laboratory of Cluster Science, Ministry of Education of China, School of Chemistry, Beijing Institute of Technology, Beijing 100081, People's Republic of China, and [‡]Department of Chemistry, Tsinghua University, Beijing 100084, People's Republic of China

ABSTRACT

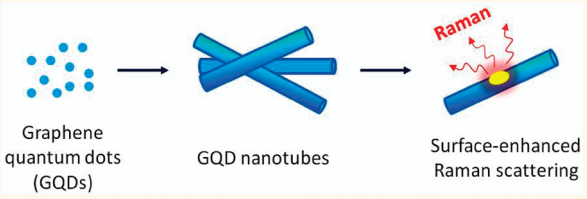

Graphene quantum dots (GQDs), single or few-layer graphenes with a size of only several nanometers, are a new type of quantum dots (QDs) with unique properties. The assembly of QDs in a geometrically well-defined fashion opens up opportunities to obtain access to the full potential of assembled QDs by virtue of the collective properties of the ensembles. In the current study, we present the well-organized assembly of zero-dimensional (0D) functional GQDs into 1D nanotube (NT) arrays and demonstrate their remarkable potential as a new metal-free platform for efficient surface-enhanced Raman scattering (SERS) applications. The hierarchically porous 1D nanotube structure of 0D GQDs has been prepared by electrophoresis deposition within a nanoporous AAO template. On the basis of the unique porous nanotube architecture of GQDs, the GQD-NTs could ensure a more efficient charge transfer between the target molecules and the GQDs and thus produce much stronger SERS effect, exceeding that on flat graphene sheets. The unique architecture of 1D nanotubes of 0D GQDs provides a new point of view for designing and fabricating SERS substrates.

KEYWORDS: graphene quantum dots · nanotube · assembly · surface-enhanced Raman scattering · template

The geometry and chemical nature of graphene nanostructures play an essential role in determining their properties as demonstrated by graphene nanoribbons and nitrogen-containing graphenes.[1−3] Graphene quantum dots (GQDs), single or few-layer graphenes with a tiny size of only several nanometers, represent a new type of quantum dots (QDs). Due to the quantum confinement and edge effects,[4−12] GQDs exhibit unique properties such as photoluminescence[4,8,13] and slow hot-carrier relaxation,[14] making them distinct from those of conventional graphene sheets. In addition to the stable photoluminescence, GQDs possess low cytotoxicity and great biocompatibility.[15] They can also overcome the extremely poor solubility and strong tendency to aggregation of graphene sheets.[12] As a consequence, GQDs present the promise for the fabrication/design of new devices with extraordinary functions. Important applications can be expected from bioimaging[15,16] to optoelectronic devices.[17−20] So far, various methods including hydro-/solvothermal route,[4,15] solution chemistry,[5,6,8,21,22] transforming C_{60} on ruthenium surface,[7] and acid treatment and chemical exfoliation of carbon fibers[23] have been developed for controllable synthesis of GQDs with specific properties and functions.[4,6,8,9,14,24] In this regard, we have recently reported a facile electrochemical approach for large scale preparation of functional GQDs,[13,25] which possess the unexpected luminescence properties, and show the potential for applications in photovoltaic cells and fuel cells.

On the other hand, assembly of QDs in a geometrically well-defined fashion opens up opportunities to control over the optical and electronic coupling between the individual QD units, which hence provides the possibility to get access to the full potential of assembled QDs by virtue of the collective properties of the ensembles.[26,27] However, the current scope of GQD study is still mainly focusing on their fundamental synthesis and primary properties. No attempt has been devoted to the use of GQDs as building blocks for fabricating functional architectures by rational arrangement. Thus, new phenomena and applications associated with the collective properties of individual GQDs remain virgin so far.

Raman spectroscopy is an important tool for structural characterization and chemical/biosensing. The development of substrates for efficiently harvesting Raman

* Address correspondence to lqu@bit.edu.cn; gshi@tsinghua.edu.cn.

Received for review November 5, 2011 and accepted February 11, 2012.

Published online February 13, 2012
10.1021/nn204289t

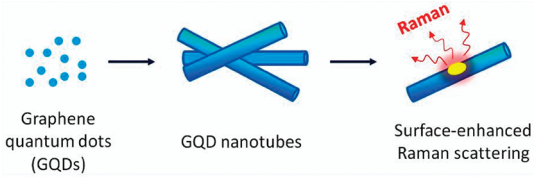

Figure 1. Scheme of the fabrication of GQD-NTs and their SERS function.

signals of target molecules has been a long-term research focus.[28] A variety of noble metals and transition metals[28−35] such as Ag, Au, Cu and Pd with rough surfaces have been conventionally used as the substrates for surface enhanced Raman scattering (SERS). However, concerning the expense, stability, (bio)compatibility and environment-friendly feature, the development of new, alternative substrates for SERS to meet the rigorous requirements is becoming of practical importance. Recently, semiconductor materials have been involved as SERS active substrates. For example, the SERS effect on InAs/GaAs quantum dots[36] and metal oxide surfaces such as ZnO,[37] TiO_2,[38] and α-Fe_2O_3[39] has already been reported. Si and Ge nanostructure arrays have also been demonstrated to have significant Raman enhancements.[40] The abundant hydrogen atoms terminated on the surfaces of Si and Ge nanoarrays play a critical role in promoting efficient charge transfers and enable the SERS effects. As a special material with crystal package of carbon atoms associated with a lot of unexpected properties,[4,7−9,14,24,41,42] graphene has exhibited the surprising promise in SERS applications.[43] The origin could be exclusively attributed to the chemical enhancement mechanism due to the fact that graphene surface is extremely smooth and highly optical transparent.[44] In this case, charge transfer is possible between the molecules and the graphene substrate, responsible for the Raman enhancement. Due to the limited surface area and the difficulty in capturing the incident light, however, only 2 to 17-fold Raman enhancement was observed on graphene film compared with SiO_2/Si substrate.[43] GQDs are the graphene sheets in quantum-scale sizes, which have much larger specific surface areas and more accessible edges comparing with those of graphene sheets. The rational assembly of GQDs into nanoporous architectures could effectively adsorb target molecules and harvest the collective Raman signals of the ensembles. As far as we are aware, however, no endeavor has been dedicated to building GQD-based architectures for SERS applications.

Recently, Li and co-workers have reported the controlled alignment of colloidal GQDs on polar surfaces through chemical functionalization.[45] Herein, we present the well-organized assembly of zero dimensional (0D) GQDs into 1D nanotube (NT) arrays, and

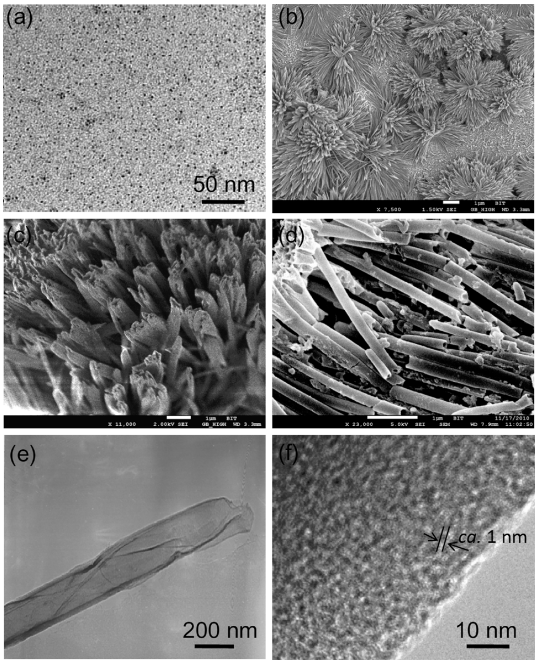

Figure 2. (a) TEM image of functional GQDs, (b−d) SEM images of assembled nanotube arrays of GQDs with different magnifications after releasing from AAO template, and (e, f) TEM images of individual GQD nanotube and its wall. (d) Deliberately broken GQD-NTs to show the hollow structure. Scale bars in (b) to (d) are 1 μm.

demonstrate their great potential as a new metal-free platform for efficient SERS applications (Figure 1).

RESULTS AND DISCUSSION

GQD-NT arrays were prepared *via* a template-assisted electrodeposition process (Figure S1). Briefly, functional GQDs were prepared by electrochemical oxidation of graphenes according to our previous report.[13] The as-prepared GQDs with a size of 3−5 nm (Figure 2a) are rich of negatively charged carboxyl groups and can be well dispersed in water, which thus provides the possibility for direct electrophoresis deposition. Au foil supported anodic aluminum oxide membrane (200-nm AAO, Whatman) acted as the working electrode. Under an applied potential of 6 V for several hours, the functional GQDs were spontaneously deposited into the nanochannels of AAO membrane to form nanotube arrays (Figure S1). Although derived from graphene dots (Figure 2a), the released GQD-NTs still remain the self-standing array structure in despite of the bundling due to the capillary effect during wet-to-dry process for removing the AAO template by 1 M NaOH treatment (Figures 2b and c). The as-formed GQD-NTs have a diameter of *ca.* 200−300 nm (Figure 2d), matching the nanopores of AAO template. Their open tips (Figure 2c) and broken sites along the length (Figure 2d) clearly show the hollow structures. Transmission electron microscope (TEM) investigation further confirms the tubular structure (Figure 2e), and reveals the as-formed nanotube is

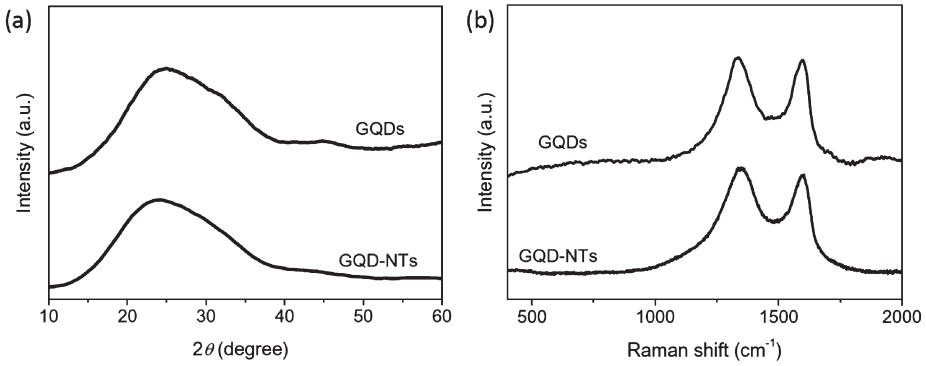

Figure 3. XRD profile (a) and Raman spectra under 632.8 nm laser (b) of GQDs and GQD-NTs.

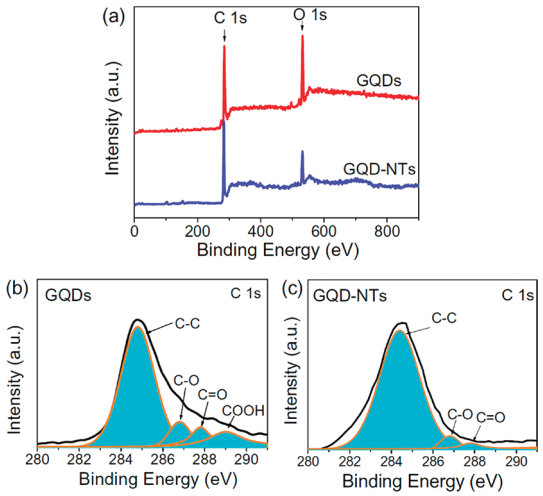

Figure 4. Overall XPS analysis of original GQDs and electrodeposition-formed GQD-NTs (a) and high resolution C 1s peaks for GQDs (b) and GQD-NTs (c).

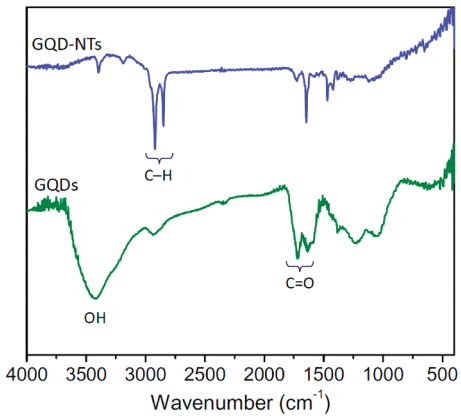

Figure 5. FT-IR spectra of functional GQDs and as-prepared GQD-NTs.

composed of uniformly sized dots (Figure 2f) in accordance with the initial GQDs (Figure 2a).[13] Although it is not accurate to determine the pore size by TEM, we can still find some gaps of *ca.* 1 nm among the assembled GQDs (Figure 2f), showing the porous structure of the tube walls.

GQDs and GQD-NTs present a similar XRD peak at *ca.* 25°, consistent with previous report (Figure 3a).[13] Raman spectra of GQD-NTs show the typical carbon-related bands located at *ca.* 1300 cm^{-1} (D band) and 1600 cm^{-1} (G band) (Figure 3b), similar to those of the initial GQDs upon the excitation with a 633 nm laser, which is also the case for using a 514-nm laser as the excitation source (Figure S2). These results indicate the electrodeposition process has negligible influence on the intrinsic crystallinity of GQDs and carbon–carbon conjugated backbones of GQDs.

X-ray photoelectron spectroscopy (XPS) was used to investigate the change of GQD components during the electrodeposition process (Figure 4). It is shown that the electrodeposition–formed GQD–NTs have a much less O percentage compared with that of original GQD precursor (Figure 4a). The O/C atomic ratio for GQDs is 26.4%, while only 11.6% O/C atomic ratio was observed for GQD-NTs, suggesting that the oxygenated groups of GQDs (e.g., hydroxyl and carboxyl groups) were significantly removed during the electrodeposition process. Accordingly, the peaks related to C–C bonds (284.6 eV) became predominant while the additional peaks of C–O (286.6 eV), C═O (288.3 eV), and COOH (289 eV) were greatly reduced (Figure 4b and c). The loss of O-related groups of GQDs makes the GQD-NTs insoluble in aqueous medium.

XPS analysis results described above are consistent with those of FT–IR spectra. As shown in Figure 5, the hydroxyl (*ca.* 3300–3600 cm^{-1}) and carbonyl groups (*ca.* 1725 cm^{-1}) related to the carboxyl groups of GQDs are drastically reduced for GQD-NTs, accompanied with the appearance of saturated C–H groups (*ca.* 2800–3000 cm^{-1}). The abundant hydrogen atoms terminated on the surface of GQDs within nanotubes could play a critical role in promoting efficient charge transfer and enable the SERS effect.[40] The electrodeposition process for forming GQD-NTs at a relatively high voltage of 6 V has effectively inspired the deoxygenization of functional groups along GQDs. This phenomenon is consistent with the observed oxidation of O-rich graphenes such as graphene oxide (GO), where GO is easily oxidized by metal salts with high oxidation potentials.[46,47] The electrons could be

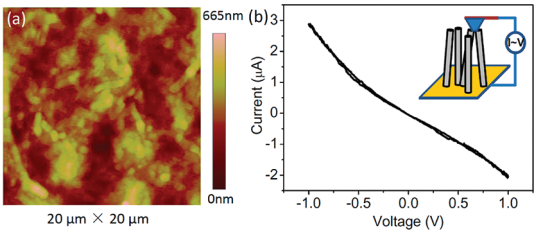

Figure 6. AFM image of GQD-NT arrays on gold film (a) and the typical *I*–*V* response based on the inset–shown setup (b). The contact area is estimated to be *ca.* 1.45 μm^2.

transferred out from GO sheets, resulting in the oxidation of GO and reducing its O content because of the release of CO_2. In current case, the O-rich GQDs are applied with a positive voltage of 6 V during electrodeposition, which is sufficiently high to oxidize the GQDs through the similar electron transfer process. As a result, a much decreased O content was observed for electrodeposition-formed GQD-NTs.

The aligned structure of GQD-NTs (Figure 6a) allows us to investigate the electronic characteristics along the length direction of nanotubes. The current–voltage (*I*–*V*) response was measured on the basis of the setup in Figure 6b (inset). A Pt-coated conducting AFM tip is placed onto the GQD–NT arrays with an applied voltage between it and the bottom gold substrate (Figure 6b, inset). The nonlinear *I*–*V* curves (Figure 6b) reveals the semiconductive behavior of the as-produced GQD–NT arrays, which is probably associated with the intrinsic semiconducting characteristic of the constituent quantum-sized graphene dots. The packed GQDs along nanotubes ensure the effective electron transport through the nanotube length. Measurements based on different contact points of GQD-NT tips exhibit the similar nonlinear I–V response to that in Figure 6b, showing the overall semimetal conductive behavior.

To explore the potential of GQD-NTs for SERS applications, we take the widely used Rhodamine 6G (R6G) as one of the model molecules. For comparison, the initial GQDs were also studied by drop-casting on the same substrate. Similar to the sample preparation for Raman investigation on grahpene sheets,[43] R6G molecules were adsorbed on GQD–NTs or GQD films by simply soaking the Si substrate supported samples in the aqueous solution of the target molecules with a certain concentration. Raman spectra were measured under ambient condition using a Renishaw microRaman spectroscope with a 632.8 nm He–Ne laser. As expected, highly enhanced Raman peaks with good signal-to-noise ratio are observed for R6G adsorbed on GQD–NTs (Figure 7a). Their vibrational frequencies are similar to those on graphene[43] and match well with those on metal-based SERS substrate reported previously (Table S1).[48–51] In contrast, no obvious Raman peaks of R6G is observed on either GQD film or Si substrate under the same conditions (Figure 7a). The

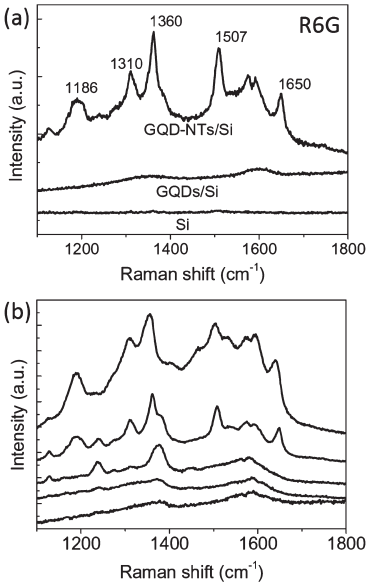

Figure 7. (a) 632.8 nm excited Raman spectra of 4×10^{-6} M R6G drop-cast on Si wafer, adsorbed on Si wafer supported GQDs (GQDs/Si) or GQD-NTs (GQD-NTs/Si). (b) 623.8 nm excited Raman spectra of R6G with different concentrations adsorbed on GQD-NTs/Si. The concentrations of R6G from bottom to up are 8×10^{-11}, 8×10^{-9}, 8×10^{-7}, 4×10^{-6}, and 4×10^{-5} M, respectively.

Raman peaks of R6G on GQD film, if any, are probably covered by the D band and G band of GQDs. These results show the unique effect of GQD assembled nanotubes for SERS. To estimate the Raman enhancement effect, we took the intensity of Raman signals of drop-casting R6G on the Si substrate as the normalization reference[43] (Figure S3). An overall 40- to 74-fold enhancement was observed on the basis of the different Raman peaks (Table S2), which is much higher than that of 2 to 17-fold enhancement on graphene film.[43] The SERS signal of R6G on GQD–NTs decreases with the decrease of R6G concentration, and the limit of detection was measured to be around 10^{-9} M at the level of single-to-noise (S/N) = 3 (Figure 7b). The Raman enhancement on GQD-NTs has also been confirmed by using a different substrate (Figure S4) or a 514.5-nm laser (Figure S5).

The large enhancement observed above suggests that these GQD-NTs can indeed serve as robust substrates for SERS. We further investigate the capability of GQD-NTs for the detection of 2,4-dinitrotoluene (2,4-DNT), the most commonly used nitroaromatic compound for buried landmines and other explosives.[52,53] Figure 8 shows a clear Raman spectrum with well-separated peaks of 2,4-DNT absorbed on the GQD–NTs. The vibrational frequencies at 1134, 1153, 1204, 1348, 1355, 1528, 1544, and 1610 cm^{-1} are consistent with the SERS results reported previously on Au and Ag substrates.[53,54] In contrast, Raman signals of 2,4-DNT on GQD film was seven times weaker in peak intensity than that on GQD-NTs and was absent of any legible fingerprint bands. Similarly, no obvious peak

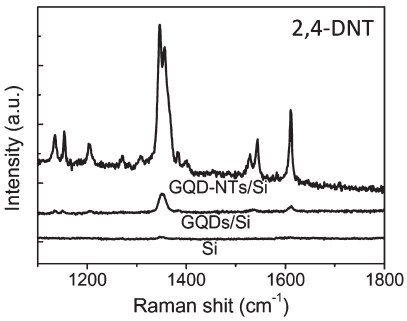

Figure 8. 632.8 nm excited Raman spectra of 2×10^{-2} M 2,4−DNT drop-casting on Si wafer, adsorbed on GQDs/Si or GQD−NTs/Si.

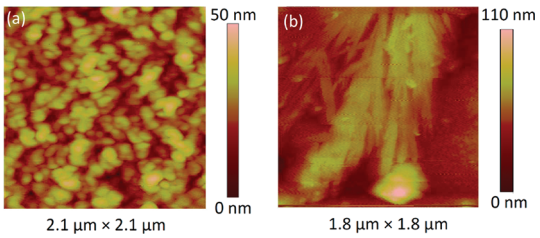

Figure 9. AFM images of the drop-casting GQD film (a) and GQD-NTs on Si wafer (b).

was observed on Si surface (Figure 8). A 59-fold Raman enhancement of GQD-NTs was obtained by comparison of the Raman intensity for the NO_2 stretching mode at 1348 cm^{-1} with that on the Si reference (Figure S6), which is consistent with the estimated enhancement from the model molecule of R6G mentioned above. These results not only further demonstrate the superior Raman enhancement on GQD−NT substrate, but also exhibit the general feature of GQD-NTs for SERS application.

Normally, the electromagnetic mechanism (EM) and chemical mechanism (CM) are widely accepted to explain the SERS effect.[55] The EM is based on the surface plasmon resonance excited by the incident light on the rough surface of a metal.[56−58] In contrast, CM is based on a charge transfer between target molecules and the substrate.[38,59−62] The previous investigations have demonstrated that the efficient charge transfer plays a critical role in activate the SERS effect for group IV materials such as carbon-based graphene,[43] Si and Ge substrates.[40] As tiny sized graphene sheets, GQDs could intrinsically have SERS effect based on CM. CM involves the close contact of target molecules with substrates, which favors the charge transfer between them and accordingly increases the Raman scattering.[43,55] Because the target molecules were directly adsorbed on the GQD surfaces, effective charge transfer could occur between them, which is supported by the observed charge transfer between graphene and the molecules.[43,63−67] In fact, the charge transfer between GQDs and organic molecules has been utilized to fabricate new-type polymer photovoltaic cells.[13] On the other hand, the chemical enhancement mechanism usually presents the vibration-dependent Raman enhancement,[40,43] which is indeed the case for GQD-NT substrate as shown in Table S2. Therefore, the SERS effect of GQDs could be provisionally attributed to the CM.

It is observed that the SERS effect on GQD-NTs is much stronger than that on GQD film (Figures 7c and 8). This difference is directly associated with the surface nature of GQDs and electrodeposited GQD-NTs since the charge transfer is strongly dependent on the surface chemistry[40] and interface interaction.[68−71] As revealed in Figures 4 and 5, the XPS and FT-IR analyses clearly indicate that the electrodeposition-formed GQD-NTs have much less O-related groups on GQDs (e.g., hydroxyl and carboxyl groups) than those of the initial GQDs. Controlled experiments show that the O-absent GQDs from electrodeposited GQD-NTs have clear Raman enhancement effect compared with the initial O-rich GQDs (Figure S7). On the other hand, the abundant hydrogen atoms terminated on the surface of GQDs could also have the potential to promote efficient charge transfer for SERS effect.[40] Considering that the SERS effect on the graphene sheet without much O functional groups is strong,[43] while it is almost absent on graphene oxides (Figure S8), we could provisionally conclude that the graphene dots in electrodeposition-formed GQD-NTs are more active for SERS effect like graphene does,[43] and the O-rich GQDs are having a tendency of impairing Raman enhancement.

We can also find that the organized GQDs within nanotube arrays provide a well-proportioned hierarchical nanoporous structure with fine rough surfaces. The porous walls plus the hollow nanostructure of GQD−NTs (Figure 2) guarantee the large surface areas for adsorption of molecules and thus effective charge transfer, and the subtle rough surfaces of nantoubes may favor the capture of the incident light for SERS. As a consequence, assembled nanotubes present intense SERS effect, while much weaker Raman signals are observed on drop-casting GQD film. This phenomenon may also imply the strong morphologic dependence of Raman spectra on GQDs, apart from the difference of surface chemistry. AFM investigation reveals the drop-casting GQD film has an irregular surface consisting of aggregated GQDs with a relatively large size of *ca.* 100−200 nm caused by the wet-to-dry process (Figure 9a). In this case, the adsorbed molecules have difficulty in forming a uniform molecule layer covering the surfaces of loosely packed GQD ensembles. In contrast, the GQD−NTs electrodeposited within AAO nanochannels remain the array structure (Figure 9b) and GQDs with a size of less than 5 nm are regularly confined in the nanotubes (Figure 2), which meet the requirement of a relatively ordered arrangement of the uniform nanoparticles for SERS.[28] On the basis of

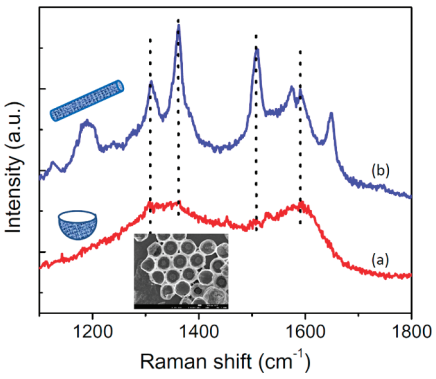

Figure 10. 632.8 nm excited Raman spectra of 4×10^{-6} M R6G adsorbed on GQD-microbowls/Si (a), and GQD-NTs/Si (b), respectively. The inset SEM image shows the as-prepared GQD microbowls with a diameter of 500 nm and a height of *ca.* 250 nm.

the unique 0D GQDs assembled 1D nanotube structure, the solution of target molecules could spontaneously infiltrate into the hollow tubular structure in virtue of the capillarity. As a result, target molecules could be uniformly enriched along nanotube length. Under laser irradiation, each of the GQDs could play a role in exciting the Raman scattering and producing a strong collective Raman signals.

To further reveal the morphological effect of GQD ensembles on SERS, we have prepared GQD microbowls (Figure 10, inset) with a much low aspect ratio of *ca.* 0.5 distinct from that of GQD-NTs (*ca.* 25) for comparison. The GQD microbowls were prepared by using the microspheres as electrodeposition template at the same condition to that for GQD-NT fabrication (Figure S9). As shown in Figure 10, the Raman signal of R6G on GQD microbowls, although better than that on drop-casting GQD film (Figure 7a), was largely minified in comparison with that on GQD-NTs. The more efficient capture of R6G molecules on GQD-NTs than GQD microbowls must play the important role in enhancing the charge transfer between target molecules and graphene dots, which is responsible for achieving the much stronger Raman signals.

CONCLUSION

In summary, GQD-NT arrays rationally assembled from functional GQDs in a geometrically well-defined fashion has been demonstrated to have remarkable Raman enhancement. Hierarchically porous 1D nanotube structure of 0D GQDs has been prepared by electrophoresis deposition within a nanoporous AAO template. The electrodeposited GQD-NTs have much less O-related groups than those of the initial GQDs, and the abundant hydrogen atoms are terminated on the surface of GQDs with GQD-NTs. Plus the unique porous nanotube architecture of GQDs, the GQD-NTs could ensure the more efficient charge transfer between target molecules and GQDs than that occurred on the flat graphene sheets, which thus produces the stronger SERS effect. The observed highly enhanced Raman signals on the 1D nanotubes of 0D GQDs provide a new angle of view for designing/fabricating SERS substrates.

EXPERIMENTAL SECTION

Preparation of GQD-NTs. GQD-NT arrays were prepared *via* a template-assisted process (Figure S1). Functional GQDs are obtained by electrochemical oxidation of graphenes according to our previous report.[13] The as-prepared GQDs with a size of 3−5 nm (Figure 2a) are rich of negatively charged carboxyl groups and can be well dispersed in water for direct electrophoresis deposition. Au foil supported anodic aluminum oxide membrane (AAO, Whatman, 200 nm) acted as the working electrode. Pt plate was used as counter electrodes. Under an applied positive potential of 6 V for 5 h, the functional GQDs were spontaneously deposited into the nanochannels of AAO membrane to form nanotube arrays although the gas bubbles were produced due to the water decomposition under the relatively high voltage. The as-prepared GQD-NTs were released by 1 M NaOH treatment for several hours.

Raman Study. Similar to the procedure of preparing the samples for Raman investigation on grahpene sheets,[43] R6G molecules were adsorbed on GQD-NTs or GQD films by simply soaking the Si substrate supported samples in the aqueous solution of the target molecules with a certain concentration. The soaking time is 2 h and the free molecules are washed with the corresponding solvent and then dried under flowing N_2. 2,4-DNT molecules were adsorbed on GQD-NTs or GQD films using the same procedure with a 2×10^{-2} M methanol solution of 2,4-DNT. One droplet of the corresponding R6G or 2,4-DNT solution was also dropped on Si substrate and used as references for Raman characterization after drying. Raman spectra were measured under ambient condition using a Renishaw microRaman spectroscopy system with a 514.5-nm argon-ion laser or a 632.8-nm He−Ne laser. The laser beam was focused by a 50 × (NA = 0.75) objective lens resulting in a spot size of around 2−5 μm in diameter. The laser power on samples was 0.47 mW for both 514.5 and 632.8 nm lasers. The acquisition time was 30 s for collecting each spectrum.

Characterizations. The morphology of the samples was examined by scanning (SEM, JSM-7500F) and transmission (TEM, JEM-2010) electron microscopes. Atomic force microscopic (AFM) images were taken using a Veeco D3100 atomic force microscope. Fourier transform infrared (FT-IR) spectra were recorded on a Bruker spectrometer (Equinox 55/S) using KBr pellets. X-ray photoelectron spectroscopy (XPS) data were obtained with an ESCALab220i-XL electron spectrometer from VG Scientific using 300W AlKα radiation. The base pressure was about 3×10^{-9} mbar. The binding energies were referenced to the C 1s line at 284.8 eV from adventitious carbon. Curve fitting of the C 1s spectra was performed using a Gaussian−Lorentzian peak shape.

Conflict of Interest: The authors declare no competing financial interest.

Acknowledgment. This work was supported by NSFC (21004006, 21174019 and 51161120361), National Basic Research Program of China (2011CB013000), and NCET-10-0047.

Supporting Information Available: Experimental setup and more Raman results (Figures S1−S9, Tables S1 and S2). This

material is available free of charge *via* the Internet at http://pubs.acs.org.

REFERENCES AND NOTES

1. Li, X.; Wang, X.; Zhang, L.; Lee, S.; Dai, H. Chemically Derived, Ultrasmooth Graphene Nanoribbon Semiconductors. *Science* **2008**, *319*, 1229–1232.
2. Wang, X.; Li, X.; Zhang, L.; Yoon, Y.; Weber, P. K.; Wang, H.; Guo, J.; Dai, H. N-Doping of Graphene Through Electrothermal Reactions with Ammonia. *Science* **2009**, *324*, 768–771.
3. Qu, L. T.; Liu, Y.; Baek, J. B.; Dai, L. M. Nitrogen-Doped Graphene as Efficient Metal-Free Electrocatalyst for Oxygen Reduction in Fuel Cells. *ACS Nano* **2010**, *4*, 1321–1326.
4. Pan, D. Y.; Zhang, J. C.; Li, Z.; Wu, M. H. Hydrothermal Route for Cutting Graphene Sheets into Blue-Luminescent Graphene Quantum Dots. *Adv. Mater.* **2010**, *22*, 734–738.
5. Xin, Y.; Xiao, C.; Li, L. S. Synthesis of Large, Stable Colloidal Graphene Quantum Dots with Tunable Size. *J. Am. Chem. Soc.* **2010**, *132*, 5944–5945.
6. Xin, Y.; Xiao, C.; Li, B. S.; Li, L. S. Large, Solution-Processable Graphene Quantum Dots as Light Absorbers for Photovoltaics. *Nano Lett.* **2010**, *10*, 1869–1873.
7. Lu, J.; Yeo, P. S. E.; Gan, C. K.; Wu, P.; Loh, K. P. Transforming C_{60} Molecules into Graphene Quantum Dots. *Nat. Nanotechnol.* **2011**, *6*, 247–252.
8. Shen, J. H.; Zhu, Y. H.; Chen, C.; Yang, X. L.; Li, C. Z. Facile Preparation and Upconversion Luminescence of Graphene Quantum Dots. *Chem. Commun.* **2011**, *47*, 2580–2582.
9. Zhao, J.; Chen, G. F.; Zhu, L.; Li, G. X. Graphene Quantum Dots-Based Platform for the Fabrication of Electrochemical Biosensors. *Electrochem. Commun.* **2011**, *13*, 31–33.
10. Zhang, H. G.; Hu, H.; Pan, Y.; Mao, J. H.; Gao, M.; Guo, H. M.; Du, S. X.; Greber, T.; Gao, H. J. Graphene Based Quantum Dots. *J. Phys.: Condens. Matter* **2010**, *22*, 302001.
11. Chen, R. B.; Chang, C. P.; Lin, M. F. Electric-Field-Tunable Electronic Properties of Graphene Quantum Dots. *Phys. E (Amsterdam, Neth.)* **2010**, *42*, 2812–2815.
12. Li, L. S.; Yan, X. Colloidal Graphene Quantum Dots. *J. Phys. Chem. Lett.* **2010**, *1*, 2572–2576.
13. Li, Y.; Hu, Y.; Zhao, Y.; Shi, G. Q.; Deng, L.; Hou, Y. B.; Qu, L. T. An Electrochemical Avenue to Green-Luminescent Graphene Quantum Dots as Potential Electron-Acceptors for Photovoltaics. *Adv. Mater.* **2011**, *23*, 776–780.
14. Mueller, M. L.; Yan, X.; Dragnea, B.; Li, L. S. Slow Hot-Carrier Relaxation in Colloidal Graphene Quantum Dots. *Nano Lett.* **2011**, *11*, 56–60.
15. Zhu, S. J.; Zhang, J. H.; Qiao, C. Y.; Tang, S. J.; Li, Y. F.; Yuan, W. J.; Li, B.; *et al.* Strongly Green-Photoluminescent Graphene Quantum Dots for Bioimaging Applications. *Chem. Commun.* **2011**, *47*, 6858–6860.
16. Alivisatos, A. P.; Gu, W.; Larabell, C. Quantum Dots as Cellular Probes. *Annual. Rev. Biomed. Eng.* **2005**, *7*, 55–76.
17. Nozik, A. J. Quantum Dot Solar Cells. *Phys. E (Amsterdam, Neth.)* **2002**, *14*, 115–120.
18. Gur, I.; Fromer, N. A.; Geier, M. L.; Alivisatos, A. P. Air-Stable All-Inorganic Nanocrystal Solar Cells Processed from Solution. *Science* **2005**, *310*, 462–465.
19. Coe, S.; Woo, W. K.; Bawendi, M.; Bulovic, V. Electroluminescence from Single Monolayers of Nanocrystals in Molecular Organic Devices. *Nature* **2002**, *420*, 800–803.
20. Tessler, N.; Medvedev, V.; Kazes, M.; Kan, S. H.; Banin, U. Efficient Near-Infrared Polymer Nanocrystal Light-Emitting Diodes. *Science* **2002**, *295*, 1506–1508.
21. Yan, X.; Li, L. S. Solution-Chemistry Approach to Graphene Nanostructures. *J. Mater. Chem.* **2011**, *21*, 3295–3300.
22. Wu, J. S.; Tomovic, Z.; Enkelmann, V.; Müllen, K. From Branched Hydrocarbon Propellers to C_3-Symmetric Graphite Disks. *J. Org. Chem.* **2004**, *69*, 5179–5186.
23. Peng, J.; Gao, W.; Gupta, B. K.; Liu, Z.; Romero-Aburto, R.; Ge, L.; Song, L.; Alemany, L. B.; Zhan, X.; Gao, G.; *et al.* Graphene Quantum Dots Derived from Carbon Fibers. *Nano Lett.* DOI: 10.1021/nl2038979.
24. Mueller, M. L.; Yan, X.; McGuire, J. A.; Li, L. S. Triplet States and Electronic Relaxation in Photoexcited Graphene Quantum Dots. *Nano Lett.* **2010**, *10*, 2679–2682.
25. Li, Y.; Zhao, Y.; Cheng, H. H.; Hu, Y.; Shi, G. Q.; Dai, L. M.; Qu, L. T. Nitrogen-Doped Graphene Quantum Dots with Oxygen-Rich Functional Groups. *J. Am. Chem. Soc.* **2012**, *134*, 15–18.
26. Murray, C. B.; Kagan, C. R.; Bawendi, M. G. Synthesis and Characterization of Monodisperse Nanocrystals and Close-packed nanocrystal assemblies. *Annu. Rev. Mater. Sci.* **2000**, *30*, 545–610.
27. Yakes, M. K.; Cress, C. D.; Tischler, J. G.; Bracker, A. S. Three-Dimensional Control of Self-Assembled Quantum Dot Configurations. *ACS Nano* **2010**, *4*, 3877–3882.
28. Lin, X. M.; Cui, Y.; Xu, Y. H.; Ren, B.; Tian, Z. Q. Surface-Enhanced Raman Spectroscopy: Substrate-Related Issues. *Anal. Bioanal. Chem.* **2009**, *394*, 1729–1745.
29. Ren, B.; Liu, G. K.; Lian, X. B.; Yang, Z. L.; Tian, Z. Q. Raman Spectroscopy on Transition Metals. *Anal. Bioanal. Chem.* **2007**, *388*, 29–45.
30. Fan, M.; Andrade, G. F. S.; Brolo, A. G. A Review on the Fabrication of Substrates for Surface Enhanced Raman Spectroscopy and Their Applications in Analytical Chemistry. *Anal. Chim. Acta* **2011**, *693*, 7–25.
31. Fleishchmann, M.; Hendra, P. J.; McQuillan, A. J. Raman Spectra of Pyridine Adsorbed at a Silver Electrode. *Chem. Phys. Lett.* **1974**, *26*, 163–166.
32. Pettinger, B.; Wetzel, H. Surface Enhanced Raman Scattering from Pyridine, Water, and Halide Ions on Au, Ag, and Cu Electrodes. *Chem. Phys. Lett.* **1981**, *85*, 473–481.
33. Ren, B.; Lin, X. F.; Yang, Z. L.; Liu, G. K.; Aroca, R .F.; Mao, B. W.; Tian, Z. Q. Surface-Enhanced Raman Scattering in the Ultraviolet Spectral Region: UV-SERS on Rhodium and Ruthenium Electrodes. *J. Am. Chem. Soc.* **2003**, *125*, 9598–9599.
34. Haynes, C. L.; Van Duyne, R. P. Dichroic Optical Properties of Extended Nanostructures Fabricated Using Angle-Resolved Nanosphere Lithography. *Nano Lett.* **2003**, *3*, 939–943.
35. Lu, G. W.; Li, C.; Shi, G. Q. Synthesis and Characterization of 3D Dendritic Gold Nanostructures and Their Use as Substrates for Surface-Enhanced Raman Scattering. *Chem. Mater.* **2007**, *19*, 3433–3440.
36. Quagliano, L. G. Observation of Molecules Adsorbed on III-V Semiconductor Quantum Dots by Surface-Enhanced Raman Scattering. *J. Am. Chem. Soc.* **2004**, *126*, 7393–7398.
37. Wang, Y. F.; Ruan, W. D.; Zhang, J. H.; Yang, B.; X, W. Q.; Zhao, B.; Lombardi, J. R. Direct Observation of Surface-Enhanced Raman Scattering in ZnO Nanocrystals. *J. Raman Spectrosc.* **2009**, *40*, 1072–1077.
38. Musumeci, A.; Gosztola, D.; Schiller, T.; Dimitrijevic, N. M.; Mujica, V.; Martin, D.; Rajh, T. SERS of Semiconducting Nanoparticles (TiO_2 Hybrid Composites). *J. Am. Chem. Soc.* **2009**, *131*, 6040–6041.
39. Fu, X. Q.; Bei, F. L.; Wang, X.; Yang, X. J.; Lu, L. Surface-Enhanced Raman Scattering of 4-Mercaptopyridine on Sub-monolayers of α-Fe_2O_3 Nanocrystals (Sphere, Spindle, Cube). *J. Raman Spectrosc.* **2009**, *40*, 1290–1295.
40. Wang, X. T.; Shi, W. S.; She, G. W.; Mu, L. X. Using Si and Ge Nanostructures as Substrates for Surface-Enhanced Raman Scattering Based on Photoinduced Charge Transfer Mechanism. *J. Am. Chem. Soc.* **2011**, *133*, 16518–16523.
41. Lin, Y. M.; Dimitrakopoulos, C.; Jenkins, K. A.; Farmer, D. B.; Chiu, H. Y.; Grill, A.; Avouris, Ph. 100-GHz Transistors from Wafer-Scale Epitaxial Graphene. *Science* **2010**, *327*, 662–662.
42. Prasher, R. Graphene Spreads the Heat. *Science* **2010**, *328*, 185–186.
43. Ling, X.; Xie, L. M.; Fang, Y.; Xu, H.; Zhang, H. L.; Kong, J.; Dresselhaus, M. S.; Zhang, J.; Liu, Z. F. Can Graphene Be Used As a Substrate for Raman Enhancement?. *Nano Lett.* **2010**, *10*, 553–561.
44. Bruna, M.; Borini, S. Optical Constants of Graphene Layers in the Visible Range. *Appl. Phys. Lett.* **2009**, *94*, 031901.

45. Hamilton, I. P.; Li, B. S.; Yan, X.; Li, L. S. Alignment of Colloidal Graphene Quantum Dots on Polar Surfaces. *Nano Lett.* **2011**, *11*, 1524–1529.
46. Zhang, N. N.; Qiu, H. X.; Liu, Y.; Wang, W.; Li, Y.; Wang, X. D.; Gao, J. P. Fabrication of Gold Nanoparticle/Graphene Oxide Nanocomposites and Their Excellent Catalytic Performance. *J. Mater. Chem.* **2011**, *21*, 11080–11083.
47. Chen, X. M.; Wu, G. H.; Chen, J. M.; Chen, X.; Xie, Z. X.; Wang, X. R. Synthesis of "Clean" and Well-Dispersive Pd Nanoparticles with Excellent Electrocatalytic Property on Graphene Oxide. *J. Am. Chem. Soc.* **2011**, *133*, 3693–3695.
48. Sun, Y. H.; Liu, K.; Miao, J.; Wang, Z. Y.; Tian, B. Z.; Zhang, L.; Li, Q. Q.; Fan, S. S.; Jiang, K. L. Highly Sensitive Surface-Enhanced Raman Scattering Substrate Made from Superaligned Carbon Nanotubes. *Nano Lett.* **2010**, *10*, 1747–1753.
49. Nie, S. M.; Emory, S. R. Probing Single Molecules and Single Nanoparticles by Surface-Enhanced Raman Scattering. *Science* **1997**, *275*, 1102–1106.
50. Michaels, A. M.; Nirmal, M.; Brus, L. E. Surface Enhanced Raman Spectroscopy of Individual Rhodamine 6G Molecules on Large Ag Nanocrystals. *J. Am. Chem. Soc.* **1999**, *121*, 9932–9939.
51. Lu, Y.; Liu, G. L.; Lee, L. P. High-Density Silver Nanoparticle Film with Temperature-Controllable Interparticle Spacing for a Tunable Surface Enhanced Raman Scattering Substrate. *Nano Lett.* **2005**, *5*, 5–9.
52. McHugh, C. J.; Keir, R.; Graham, D.; Smith, W. E. Selective Functionalisation of TNT For Sensitive Detection by SERRS. *Chem. Commun.* **2002**, 580–581.
53. Tao, A.; Kim, F.; Hess, C.; Goldberger, J.; He, R. R.; Sun, Y. G.; Xia, Y. N.; Yang, P. D. Langmuir–Blodgett Silver Nanowire Monolayers for Molecular Sensing Using Surface-Enhanced Raman Spectroscopy. *Nano Lett.* **2003**, *3*, 1229–1233.
54. Sylvia, J. M.; Janni, J. A.; Klein, J. D.; Spencer, K. M. Surface-Enhanced Raman Detection of 2,4-Dinitrotoluene Impurity Vapor as a Marker To Locate Landmines. *Anal. Chem.* **2000**, *72*, 5834–5840.
55. Campion, A.; Kambhampati., P. Surface-Enhanced Raman Scattering. *Chem. Soc. Rev.* **1998**, *27*, 241–25.
56. Moskovits, M. Determination of the Wave Field from Scattering Data. *Rev. Mod. Phys.* **1986**, *57*, 783–786.
57. Braun, G.; Pavel, I.; Morrill, A. R.; Seferos, D. S.; Bazan, G. C.; Reich, N. O.; Moskovits, M. Chemically Patterned Microspheres for Controlled Nanoparticle Assembly in the Construction of SERS Hot Spots. *J. Am. Chem. Soc.* **2007**, *129*, 7760–7761.
58. Svedberg, F.; Li, Z. P.; Xu, H. X.; Käll, M. Creating Hot Nanoparticle Pairs for Surface-Enhanced Raman Spectroscopy through Optical Manipulation. *Nano Lett.* **2006**, *6*, 2639–2641.
59. Persson, B. N. J.; Zhao, K.; Zhang, Z. Y. Chemical Contribution to Surface-Enhanced Raman Scattering. *Phys. Rev. Lett.* **2006**, *96*, 207401.
60. Lombardi, J. R.; Birke, R. L.; Lu, T.; Xu, J. Charge-Transfer Theory of Surface Enhanced Raman Spectroscopy: Herzberg–Teller Contributions. *J. Chem. Phys.* **1986**, *84*, 4174–4180.
61. Lombardi, J. R; Birke, R. L. A Unified Approach to Surface-Enhanced Raman Spectroscopy. *J. Phys. Chem.* **2008**, *112*, 5605–5617.
62. Albrecht, A. C. On the Theory of Raman Intensities. *J. Chem. Phys.* **1961**, *34*, 1476–1484.
63. Xie, L. M.; Ling, X.; Fang, Y.; Zhang, J.; Liu, Z. F. Graphene as a Substrate To Suppress Fluorescence in Resonance Raman Spectroscopy. *J. Am. Chem. Soc.* **2009**, *131*, 9890–9891.
64. Das, B.; Voggu, R.; Rout, C. S.; Rao, C. N. R. Changes in the Electronic Structure and Properties of Graphene Induced by Molecular Charge-Transfer. *Chem. Commun.* **2008**, 5155–5157.
65. Lu, Y. H.; Chen, W.; Feng, Y. P.; He, P. M. Tuning the Electronic Structure of Graphene by an Organic Molecule. *J. Phys. Chem. B* **2009**, *113*, 2–5.
66. Wehling, T. O.; Novoselov, K. S.; Morozov, S. V.; Vdovin, E. E.; Katsnelson, M. I.; Geim, A. K.; Lichtenstein, A. I. Molecular Doping of Graphene. *Nano Lett.* **2008**, *8*, 173–177.
67. Manna, A. K.; Pati, S. K. Tuning the Electronic Structure of Graphene by Molecular Charge Transfer: A Computational Study. *Chem. Asian J.* **2009**, *4*, 855–860.
68. Guo, C. X.; Yang, H. B .; Sheng, Z. M.; Lu, Z. S.; Song, Q. L.; Li, C. M. Layered Graphene/Quantum Dots for Photovoltaic Devices. *Angew. Chem., Int. Ed.* **2010**, *49*, 3014–3017.
69. Guo, C. X.; Li, C. M. A Self-Assembled Hierarchical Nanostructure Comprising Carbon Spheres and Graphene Nanosheets for Enhanced Supercapacitor Performance. *Energy Environ. Sci.* **2011**, *4*, 4504–4507.
70. Guo, C. X.; Wang, M.; Chen, T.; Lou, X. W.; Li, C. M. A Hierarchically Nanostructured Composite of MnO_2/Conjugated Polymer/Graphene for High-Performance Lithium Ion Batteries. *Adv. Energy Mater.* **2011**, *1*, 736–741.
71. Guo, C. X.; Zheng, X. T.; Lu, Z. S.; Lou, X. W.; Li, C. M. Biointerface by Cell Growth on Layered Graphene–Artificial Peroxidase–Protein Nanostructure for in Situ Quantitative Molecular Detection. *Adv. Mater.* **2010**, *22*, 5164–5167.